

Student Name Lynn van Rooijen-McCullough

HET625

Student ID 6493661

Project Supervisor Arthur Coombs

SAO Project Cover Page

Project 100

Deep imaging with a CCD and Telescope

All of the work contained in this project is my own original work, unless otherwise clearly stated and referenced.

I have read and understood the SAO Plagiarism Page “What is Plagiarism and How to Avoid It” at

<http://astronomy.swin.edu.au/sao/students/plagiarism/>

Project 100 - Deep imaging with a CCD and Telescope *Lynn van Rooijen-McCullough*

Abstract

Using an amateur 11" SCT reflecting telescope with Hyperstar lens, producing an $f/2$ focal ratio, more than 20 hours of deep sky images of two rich fields in the Virgo Galaxy Cluster were obtained. After selection, this resulted in two final images: 8 hours centered on M86 and 3.5 hours, centered on M58. Comparison of magnitudes obtained from these images with published magnitudes showed generally good agreement, particularly up to magnitude 20 and $z \approx 0.35 - 0.40$. While above that level, it was still possible to correctly identify the galaxies up to magnitude 22 – 23 and $z \leq 0.7$, particularly above magnitude 21.5, measurement errors increased as S/N ratios decreased. The 3.5-hour M58f image showed good agreement with both the published magnitudes and the results of the 8-hour M86f image through magnitude 19 – 20, but showed a wider variance from published magnitudes at magnitudes >20 . Differences in morphology among the galaxies were discernable through magnitude 17 – 18.

1 Introduction

In recent years, amateur telescopes and imaging equipment have achieved results that 25 - 30 years ago could only be obtained with meter-diameter telescopes. This project explores the limits of what can be achieved with a modest amateur set-up comprised of an 11" SCT reflector telescope and a one-shot-color CCD camera. In particular, the magnitude limits achievable with exposure times of several hours will be examined, as well as factors influencing the quality and accuracy of these measurements. In order to do this, it was desirable to image a galaxy cluster that had been well studied and also contained fields with a wide sample of galaxies, varying both in magnitude and distance.

As our nearest galaxy cluster, the Virgo Cluster has been one of the most well-studied galaxy clusters. Measurements of this cluster in the 1930's led astronomers to suggest for the first time the existence of some sort of "dark matter" (Smith 1936; Zwicky 1937). The Virgo Cluster is known to have more than 2000 members (Binggeli et al. 1985; Lopes 2007). There are several prominent giant

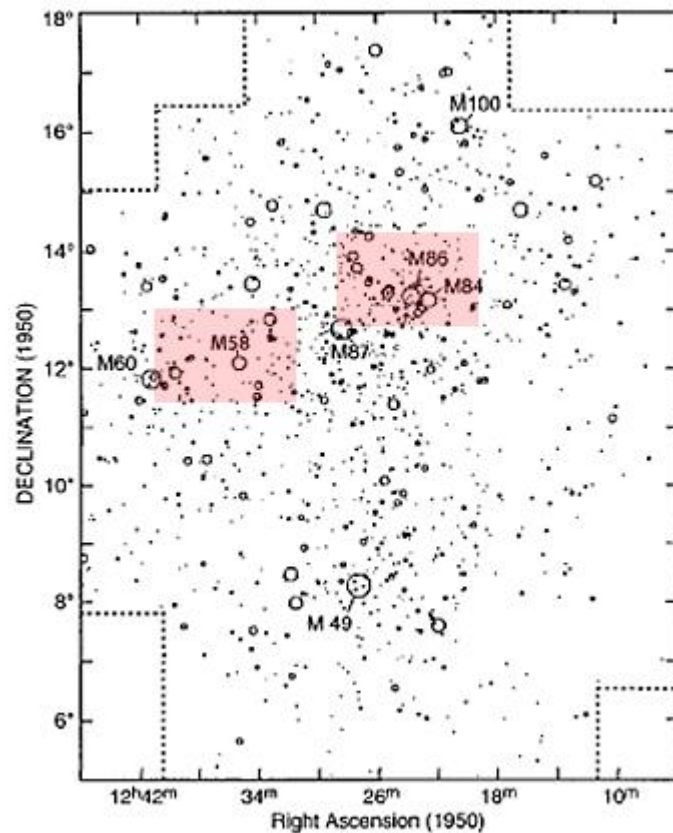


Fig. 1: Overview of Virgo Cluster with selected fields highlighted in red. Credit: Binggeli & Huchra (2001)

elliptical galaxies, including M87, which is considered to mark the center of the cluster. However, the majority of the cluster members are dwarf ellipticals which are often found in swarms around the larger, more massive ellipticals. Distance estimates have been calculated using various standard candles including Cepheids (Sandage & Tammann 2006), supernovae, planetary nebulae (Ciardullo et al. 1989) and globular clusters (Villegas et al. 2010). Although estimates range from 15 – 21 Mpc, the most generally accepted distance to the Virgo Cluster is $\approx 16 - 17$ Mpc. The diameter of the cluster is ≈ 7 Mpc.

Our own Local Group is gravitationally influenced by this cluster, which has reduced our movement away from the cluster by $\sim 250 \text{ km s}^{-1}$ compared to the normal expansion rate of the Universe. A 3-dimensional model of the cluster can be developed by measuring the recessional velocities of individual cluster members. These vary from blue-shifted velocities of up to $\sim 730 \text{ km s}^{-1}$ for galaxies moving toward the center of the cluster from behind it, to rates of $> 2500 \text{ km s}^{-1}$, more than twice the Hubble flow, for galaxies moving toward the center of the cluster from locations between us and the center.

The cluster has two main groups, the largest group, centered on M87, and a smaller cluster, centered on M49, as well as two possible sub-groups near M60 and M100. There appear to be concentrations along two axes, with the M86/84 – M87 M60 axis lining up with the jet axis of active galaxy M87. The two fields chosen for this project are highlighted in red in Fig. 1, and lie roughly along this axis. However, there is evidence that galaxies also extend beyond the cluster along a filament reaching in the direction of the “W-cloud”, twice the distance of the Virgo Cluster, and perhaps even further, to the so-called “Great Wall” (Binggeli & Huchra 2001). Because of this diversity, a deep-field image of this area can show not only the relatively close members of the Virgo Cluster, but also more distant galaxies at redshifts up to $z \sim 0.7 - 0.8$, making this a particularly interesting area to target.

Section 2 discusses the equipment and observing location. Section 3 outlines the collection, reduction and measurement procedures as well as the catalogues used for comparison. Section 4 discusses the results and section 5 summarizes the conclusions and gives ideas on improving results and possible future directions of inquiry. The Appendix contains an overview of the reduction log, the final color images and a number of larger images of the thumbnail images contained in the body of the paper.

2 Equipment & observing location

2.1 Telescopes

2.1.1 Main Telescope

The imaging telescope was an 11"/280mm, 2800 mm focal length, $f/10$ Celestron Nexstar GPS SCT with StarBright XLT coatings. Its limiting visual magnitude is nearly 15 (Celestron-web). The Nexstar is a fork-mounted, alt-az oriented SCT. For astrophotography, the Celestron heavy-duty wedge is used to facilitate equatorial alignment and tracking. On this model, the secondary mirror can be removed and the imaging equipment placed at prime focus, reducing the focal ratio to a very fast $f/2$.

2.1.2 Finder/Guide telescope

The finder/ guide telescope was a Stellarvue Nighthawk 80ED, an 80 mm, 560 focal length $f/7$ doublet refractor with extra low-dispersion glass (Stellarvue-web). Extreme broadband multicoatings are used on all four air-to-glass surfaces to help produce extremely sharp images. Its focal length is nicely matched to that of the main telescope.

2.2 Hyperstar lens

Celestron first introduced the Fastar system in 1997 on an 8" SCT, but the early models suffered from various types of aberration. In 2001, the Fastar system was introduced for the 11" Nexstar GPS. However, Starizona currently manufactures all Hyperstar lenses for both Meade and Celestron telescopes. Since 2001, the Hyperstar has been significantly improved, resulting in the current Hyperstar 3 model (see Fig. 2).

Inserted in place of the secondary, the Hyperstar lens is actually a field corrector instead of a focal reducer. Placing the camera at prime focus introduces aberrations that are normally corrected by the secondary, particularly spherical aberration. However, the Hyperstar is designed to correct for this as well as coma, astigmatism, chromatic aberration and field curvature. The distance to the focal plane is very critical. The Hyperstar 3 is compatible with 27mm sensors, and has the ability to rotate the camera without disturbing the rest of the assembly, and the ability to be collimated. This is important since the primary mirror of the telescope is not always perfectly orthogonal to the optical axis (Tucker 2008), although this is a very sensitive and somewhat error-prone procedure.



Fig 2: Celestron SCT with Hyperstar lens & Starlight Xpress CCD attached. Credit: Starizona-web

Advantages of the Hyperstar set-up are the fast $f/2$ focal ratio, which is 25 times faster than $f/10$, and the wide field of view. The greatest disadvantage of this system is that the camera must be removed to switch filters, which are screwed into the Hyperstar's adaptor. This can introduce dust, and often slightly changes both the orientation and focus of the camera. With the Hyperstar lens, the focal length becomes 560 mm. The lens itself creates no additional central obstruction and weighs approximately 1 kg. In order to balance the weight of the front-end camera and lens, an additional counterweight is inserted at the rear of the telescope, in place of the diagonal.

2.3 Imaging & Guider CCDs

The imaging camera was a Starlight Xpress SXVF-M25c (hereafter M25c), an APS sized, one-shot color CCD based on the Sony ICX413AQ SuperHAD chip (Starlight-web). The diameter of the M25c is similar to that of the secondary mirror opening, creating no additional central obstruction during imaging. The dark noise is exceptionally low and the chip itself is free from major defects. The autoguider was an ATiK 16iC monochrome CCD camera, which utilizes a significantly smaller, but very sensitive chip, allowing guide stars to be found even in sparsely populated fields (ATiK-web). See Table 1 for further specifications.

This combination of telescope and CCD images a field of $2.4^\circ \times 1.6^\circ$. The linear size of a stellar image with 2 arcsec seeing at $f/2$ is only 5.4 microns, although at $f/6.3$ and $f/10$, the ideal size is 17.1 and 27.1 microns respectively. Using the Nyquist criterion, which holds that the stellar image should fall on at least two pixels, this presents a problem when imaging at $f/2$, since a pixel of 2.7 microns would be required. At $f/6.3$ the preferred size would be 8.6 microns and at $f/10$, 13.6 microns.

Specifications	Starlight M25C CCD	Lodestar Guider
Pixel Array	3024x2016	640 x 480
Pixel Array in mm	23.4 x15.6 mm	7.52 x 5.80 mm
Pixel Size	7.8 μm	7.4 μm
Total effective	6.1 megapixels	0.31 megapixels
Sensor type	Sony ICX413AQ SuperHAD CCD	Sony ExView ICX429AL interline CCD
Data Format	16 bit	16 bit
Spectral response	QE peak 540nm (60%), 50% 400nm & 650nm	QE peak 620nm (65%), 35% 400nm & 770nm
System Gain	0.4 e- per ADU	0.9 electrons per ADU
Readout Noise, e-	< 12 e- RMS, ave. 7 e- RMS	7 e- RMS
Full Well Capacity	> 25000 e- (unbinned)	> 50,000 e- (unbinned)
Cooling	Single stage TEC up to 30°C below ambient	Peltier air cooling

Table 1: Specifications imaging camera and autoguider. Sources: Starlight-web & ATiK-web

If the seeing is exceptional, this ideal size would be reduced to 1.3 microns at $f/2$, a size which does not exist in amateur CCDs. 5.4 microns is near the lowest limit available. In addition, the CCD also needs to function at $f/6.3$ and even at $f/10$ on occasion. In this light, the 7.8 micron pixels of the M25c are a good general compromise for this set-up, but produce some undersampling at $f/2$. However, the advantages of fast-imaging at $f/2$, together with the wide field of view, generally outweigh this disadvantage.

2.4 Observing location

Imaging was done at Domaine de Pradines, near Lanuejols (Gard), France, RA 3.18E, dec 44.18, altitude $\pm 1000\text{m}$, between April 9th and April 18th, 2010. This site is far removed from any major cities and has an unobstructed view in all directions except for a small hill on the north side (see Fig. 3).

The sky brightness, measured at the zenith with a sky meter on various nights, ranged from ~ 21.3 to 21.6 (van Gastel, J. 2010). Moisture levels varied and there was noticeable extinction from dust near the horizon. However, images for this project were taken while objects were within 30° of the zenith, minimizing most of these problems.



Fig. 3: Imaging set-up in France, Celestron 11", getting ready to take flat-fields.

2.5 Software

MaximDL Pro was used for image capture and autoguiding (Maxim-web). MiraPro 7 (Mira-web) was used to create master calibration frames, although Maxim can also be used for this task. However, because these images were bayered and Mira cannot yet debayer, color-conversion had to be done in Maxim. Photometry was done with Mira, because, in contrast to MaximDL, MiraPro has the ability to convert an image to RA-dec coordinates /World Coordinate System (WCS) and import external catalogues for measurement. Color images were finished in Adobe Photoshop CS4.

3 Data Collection, Data Reduction & Comparison Catalogue Data

3.1 Choice of fields

One primary (Fig. 4) and one secondary (Fig. 5) field were chosen for this project. The primary field was centered on Markarian's Chain (hereafter M86f refers to this entire field, unless otherwise noted), which contains a wide range of objects from giant ellipticals and dwarf members of the Virgo Cluster to distant background galaxies, known as luminous red galaxies (LRGs) at $z \leq 0.7$. This same field had been imaged a year earlier, but for a much shorter time, and so this provided some basis for comparison.



Fig. 4: The M86f field, centered on M86 Markarian's Chain.



Fig. 5: The M58f field, centered on M58.

The secondary field is roughly centered on M58 (hereafter M58f refers to the entire M58 field). Although not originally planned, cooperation of both weather and equipment allowed for an early completion of the M86f data collection, and so this second field which has fewer large, luminous galaxies, was imaged as a comparison for the longer exposure of the M86f field.

3.2 Data collection procedures

3.2.1 Calibration frames

Bias, dark and flat frames were utilized for calibration. Bias frames were collected on the first evening. Dark frames were collected both before and after two different imaging sessions, with exposure times matching each of the light exposure times. This series represented the typical temperature range during

the imaging sessions. Since this CCD is relatively noise-free and the average nightly temperature was a low 1 - 4° C, the temperature variation during and among the evening(s) was not critical. Flat fields were collected at twilight with an average pixel saturation of 50%. Inspection showed few dust artifacts and so the flats primarily functioned to correct vignetting. Since no filters were used, only one set of flats was necessary.

3.2.2 Light frames

Light frames were collected for M86f between April 9 – 14th. However, inspection showed that although the initial images were adequate, the Hyperstar was not precisely collimated during the first two nights. The following nights provided 8 additional hours of good images and so the data from the first 2 nights were ultimately not used after a comparison of the results of a 43,000s image with the total of all nights but with small collimation distortions in the lower half did not produce a significantly better quality image than the images used for this project. Narrowband images of M86f were taken on two subsequent nights, and will be used for a subsequent project. M58f was imaged on April 17th and 18th.

Exposures were taken at 60s, 120s, 240s, 300s, and 480s. 480s pushes the tracking limit of the mount/wedge combination if there is any wind, and satellite trails were a hindrance during the early part of the evenings, making a combination of shorter exposures prudent. These shorter exposures also avoided saturating the pixels of all but the brightest stars and so reduced measurement errors that could have been caused by non-linearity of response and the use of an anti-blooming CCD. The majority of the exposures were 240s and 300s for both fields.

3.3 Reduction procedure

The first part of the reduction process entailed calibrating the individual images, which were not yet debayered. To do this, it was first necessary to create a Master Bias frame, one Master Dark frame per exposure time and a Master Flat frame. The M25c CCD does not contain an overscan region and so overscan subtraction could not be applied. Detailed procedures and logs can be found in Appendix 7.1. The general procedure used in Mira was as follows:

- Create Master Bias using Mean combine
- Create Master Darks per exposure time: subtract bias, combine using Median
- Create Master Flat: subtract bias, subtract dark, combine using Median combine, normalize to 1

Because of the inability of Mira to debayer, it was necessary to finish calibration in MaximDL. Tests were run to determine at what point to make the transition to MaximDL to obtain optimal results: reducing images in Mira, with debayering and combining in Maxim, or performing reduction, debayering and image combination in Maxim. The results showed no significant difference between the two procedures. Therefore, MaximDL was chosen for the entire procedure because of its flexibility in combination routines.

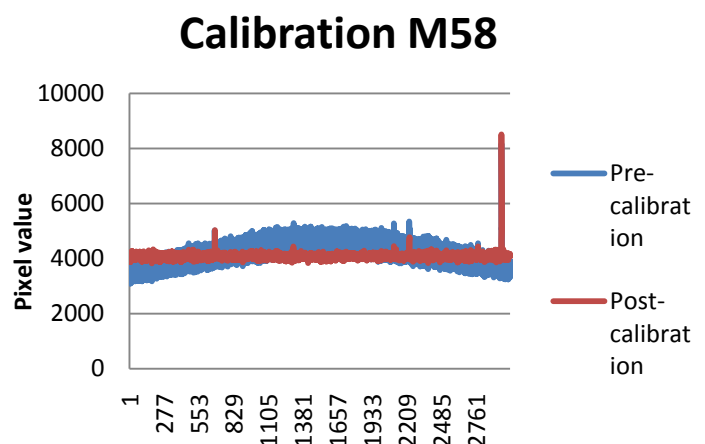


Fig. 6: Typical image, before and after calibration.

The Master Calibration frames were then used to calibrate each of the images in MaximDL. The procedure was as follows:

- Subtract the Master Bias frame from each image
- Subtract the appropriate exposure Master Dark from each image
- Divide the Master Flat into each image
- Debayer
- Combine images according to chosen algorithm.

This process was run separately per image for each field. In the case of the M58 data shown in Fig.6, and representative of a typical image, calibration successfully flattened the image and reduced the standard deviation within various background selections by 50%.

The images per field were combined both by simple summing and by using Sigma Clipping or Standard Deviation Masking algorithms. These last two techniques remove outlier pixels and then average the remaining pixels. In this way, they combine the noise reduction advantages of an average combine with the outlier pixel rejection of median combine, but if applied too aggressively, can also remove faint data or introduce artifacts. The final M86f image consisted of 124 exposures of 231 seconds average, for a total of 28644 seconds or ≈ 8 hours. The M58f image combined 49 images with an average exposure of 254 seconds for a total of 12460 seconds, or $\approx 3 \frac{1}{2}$ hours total. The standard deviation of the background of the M86f was only 3.858 at a background level of 2907, while the standard deviation of the M58f was 6.3 at a background level of 2304. The slight difference probably reflects the result of the longer exposure and larger number of images used for the M86f field.

The resulting images then followed two different paths per image. One version of the image was converted to monochrome in order to measure the galaxy magnitudes in MiraPro. The second was stretched in MaximDL to bring out detail in the lower brightness ranges, and adjusted with slight application of levels to balance color and other minor adjustments to form the finished color images seen in Fig. 4 & 5 and in Appendix 7.2. Even without any analysis, it was apparent that compared to the previous year's shorter image, the new, longer exposure of the M86f image contained both more detail in the brighter galaxies, including both color and features such as dust lanes, and a much larger number of fainter stars and galaxies.

3.4 Data and sample selection

3.4.1 Catalogues

Because it was not possible to image using photometric filters and/or with a non-anti-blooming, monochrome CCD camera, a creative solution was necessary for measuring and comparing magnitudes with published results. Any results obtained can therefore only be considered to be magnitude estimates, representing a general range.

To reduce the uncertainties of the results, and to explore different aspects of the images, measurements were compared to four different catalogues. The first was the well-known Virgo-Coma Cluster Catalogue (VCC) of more than 2000 galaxies (Binggeli et al. 1985). This catalogue includes magnitudes between $\approx 12 - 20$. These are film images taken with the 2.5m du Pont reflector at Las Campanas, some with use of an UV-cutoff filter. Magnitudes were visually estimated based on a catalogue of 109 standard galaxies, and so these magnitudes were expected to be comparable to the

monochrome image. To examine the effects of greater distance, galaxies taken from SDSS data release 5 with similar magnitudes but covering $z = 0.009$ to 0.2 , with an average of $z = 0.12$, were also measured (Tago et al. 2008).

Because this project is primarily concerned with determining the limits of the telescope-imaging combination, another catalogue was needed to extend the magnitude range. Two other catalogues were ultimately used. The MegaZ-LRG survey (Collister et al. 2007) covers LRGs with redshifts of $z = 0.4$ to 0.7 from SDSS data release 4 (Adelman-McCarthy et al. 2006). Galaxies within the target areas generally had measured g magnitudes of between $18.5 - 23.0$. A second LRG catalogue (Lopes 2007), using SDSS data release 5 (Adelman-McCarthy et al. 2007) and employing more stringent selection criteria in both color and magnitude to reduce possible stellar contamination, was also used. This catalogue included some galaxies as bright as magnitude 15 and so provided a longer continuum for the measurements than Collister et al. 2007.

In addition to measuring only magnitude, it was of interest to see to what distances and magnitudes some hints of galaxy morphology could be detected with the imaging set-up. The galaxies selected from Binggeli et al. (1985) were all be classified as elliptical or dwarf elliptical. However, two other papers/catalogues provided a richer variety (Lisker et al. 2006, 2007) and this data was used to examine the morphology of the fainter galaxies.

Selections were made from all catalogues based on the known RA-dec coordinates of the two fields. In addition, galaxies brighter than ≈ 15 were generally excluded since they were too bright to be accurately measured by aperture photometry targeted at the fainter galaxies. After tests showed that the magnitude uncertainty of galaxies fainter than $\approx 22 - 23$ was too great, these were also excluded from the samples.

3.5 SDSS filters

With the exception of Binggeli et al. (1985), all of the catalogues employed data from the SDSS surveys, which utilize the Sloan u-g-r-i-z system. Fig. 7 compares an approximation of the response of the M25c CCD with that of the various Sloan filters. No single filter matches the CCD, but the g filter has the most similarity. For most catalogues, a triple approach was used: primary comparison was the g filter, second the r , and third, a weighted average containing $3x g$ and $2x r$, which more closely approximates CCD response, as described in section 4.4.

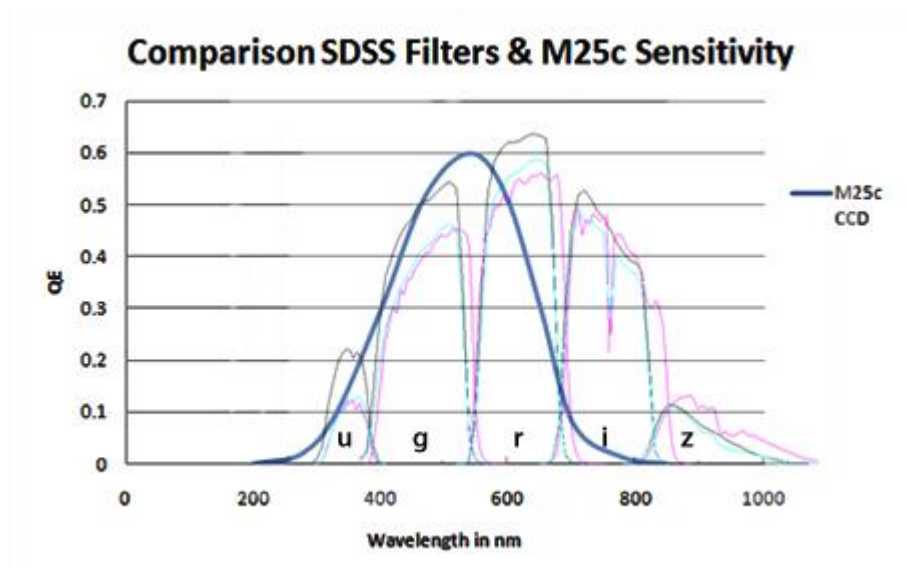


Fig. 7: Comparison of estimated response of the M25c CCD compared to the passbands of the SDSS filters. SDSS curves credit: SDSS-filter-web

3.6 Photometry procedure

In order to locate large numbers of known galaxies in an image, particularly faint objects, it is useful to convert an image to WCS coordinates. This astrometric calibration was performed in MiraPro on all of the monochrome images used for the photometry. The procedure was successful, with an uncertainty of only 0.1289 arcsec in RA and 0.0485 arcsec in dec for M86. Since the image scale was calculated to be 2.85 arcsec/pixel, this result was certainly accurate enough for the purposes of this project.

Second, a zero-point, the magnitude at which an object produces one count per second, had to be determined in order to convert raw signal to magnitude, using the formula $m = -2.5 \times \log_{10}(\text{GAIN} * \text{COUNT} / \text{EXPTIME}) + \text{ZEROPOINT}$. Initially, a zero point was determined using 10 – 15 stars of known visual magnitude per image. The stellar-based zero-point for M86f was 20.1905. For M58f, it was 19.11. The reason for this difference was not immediately apparent.

However, stars are more point-like sources than even many of the smaller galaxies and so a second zero point was also determined based on measurements of 18 VCC galaxies per image. This second technique produced galaxy magnitudes slightly more in line with the g magnitudes. However, while a different zero point linearly affects the magnitudes, it does not affect the slope of the measured galaxies compared to g magnitudes. The effect of using the galaxy zero point instead of the stellar zero point (reduction of 0.17 magnitudes in the case of M86f) can be simply calculated and applied to all images when relevant.

On the other hand, the galaxy calculated zero-point for M58f increased from 19.11 to 20.16, which is more in line with the M86 zero-point. This result was recalculated and reconfirmed the new result, perhaps indicating an error or bias in the original star-based zero-point calculation. After applying the WCS coordinates, the galaxy selections were then uploaded to MiraPro, which marked the galaxies as shown in Fig 8.

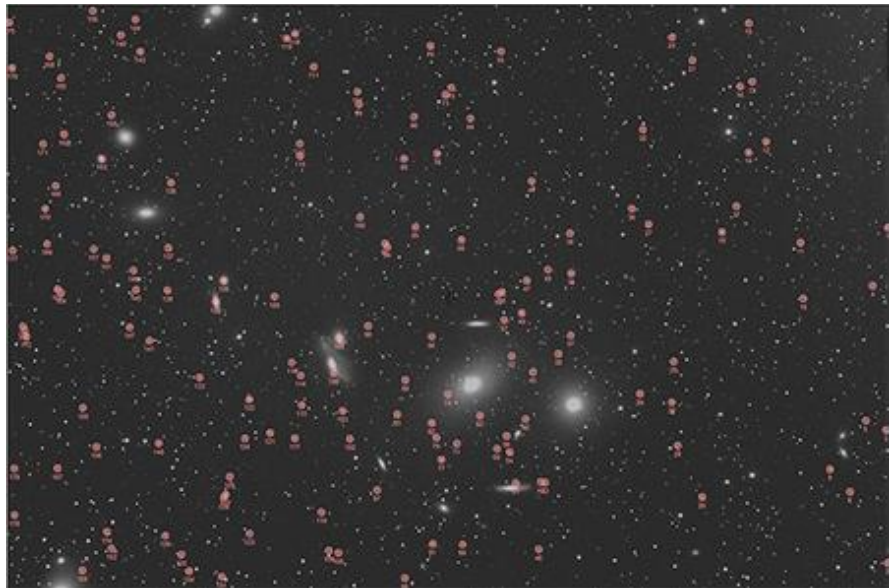


Fig. 8: Example of an image with positions of catalogue galaxies marked in red.

Initial selections per catalogue contained 150 – 450 galaxies per field. Depending on the magnitude range of the galaxies to be measured, a central aperture of 4 or 5, with inner and outer apertures at 8 – 12 or 10 – 15 respectively per image was used. Several sources of potential error led to most of the selections being reduced by half or more. The fields were crowded and a bright star often contaminated the measurements in the outer annulus. Mira often locked onto a bright foreground star adjacent to a fainter galaxy, which would have contaminated the aperture even if Mira could have locked onto the fainter galaxy. Also, many fainter, more distant, galaxies occurred in groups of two or more, and were too small to be separated and accurately measured. Last, particularly for galaxies measuring fainter than magnitude 21, a visual check was necessary to assess whether a signal and not simply a peak in

random noise was being measured, especially when measuring near the edges of the image which tended to be slightly noisier than the central area. This rigorous selection probably eliminated some valid galaxies, but it was thought better to err on the conservative side.

4 Results

4.1 VCC catalogue galaxies

The final VCC selection from Binggeli et al. (1985) for M86f contained 85 galaxies with VCC magnitudes between 15 – 20. The M58f selection contained 74 galaxies between mag 11- 20. As Fig.9 shows, the agreement between the given VCC magnitudes and the measured magnitudes for both fields was generally excellent, with higher errors primarily at the fainter end. In both cases, measured values were slightly higher (fainter) for the brighter galaxies and lower (brighter) for fainter magnitudes, relative to catalogue magnitudes.

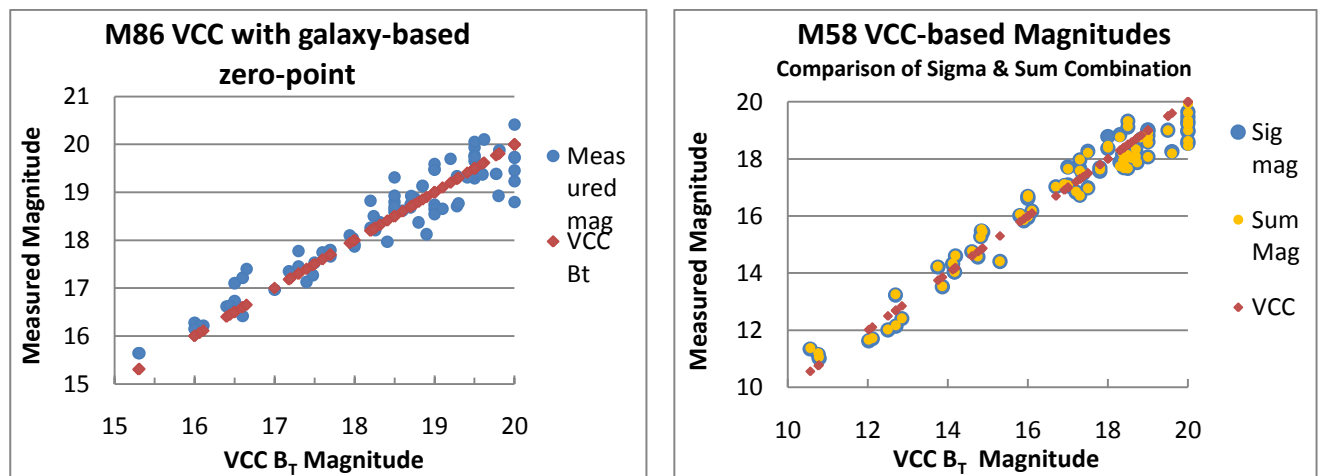


Fig. 9: Comparison of measured magnitudes with VCC B_T magnitudes for both fields.

This could have been caused by the use of the aperture, which would have missed some of the light from the larger/brighter galaxies, while the original VCC magnitudes were determined by visual comparison and less hindered by this problem.

A second conclusion was that measurements produced by summed and averaged images did not differ significantly from one another, as shown by the M58f charts in Fig. 9 & 10. Since the sigma-clip method removes or at least lessens satellite trails and other incidental defects which could affect measurements, the sigma-clip combined images were used for further analysis.

4.2 Tago et al. (2008)

The Tago et al. (2008) catalogue was interesting to compare to the VCC catalogue data as it contained larger samples for both fields which were measured with Sloan photometric filters. The M86f field contained 264 galaxies after removal of the most contaminated annuli, while the M58f field contained 176. Again, a comparison of the summed image and the averaged image showed no significant differences in measurement results. Both the M86f and M58f fields showed good agreement in terms of slope (see Fig. 10), although a similar but weaker trend was still seen, similar to that seen in the VCC measurements, of fainter measurements at brighter magnitudes and brighter at the fainter magnitudes

compared to the catalogue values. This was initially surprising since this catalogue contains many more distant background galaxies than the VCC catalogue, which could be expected to appear relatively fainter due to extinction and might even be beyond the range of the imaging set-up, and so required further investigation.

However, based on both VCC and Tago results, it can be concluded that at magnitudes brighter than $\approx 19 - 20$, galaxies in both the M86f and M58f fields can be captured, correctly identified, and relatively accurately measured with amateur equipment, despite the differences in the M86f / M58f in total exposure times.

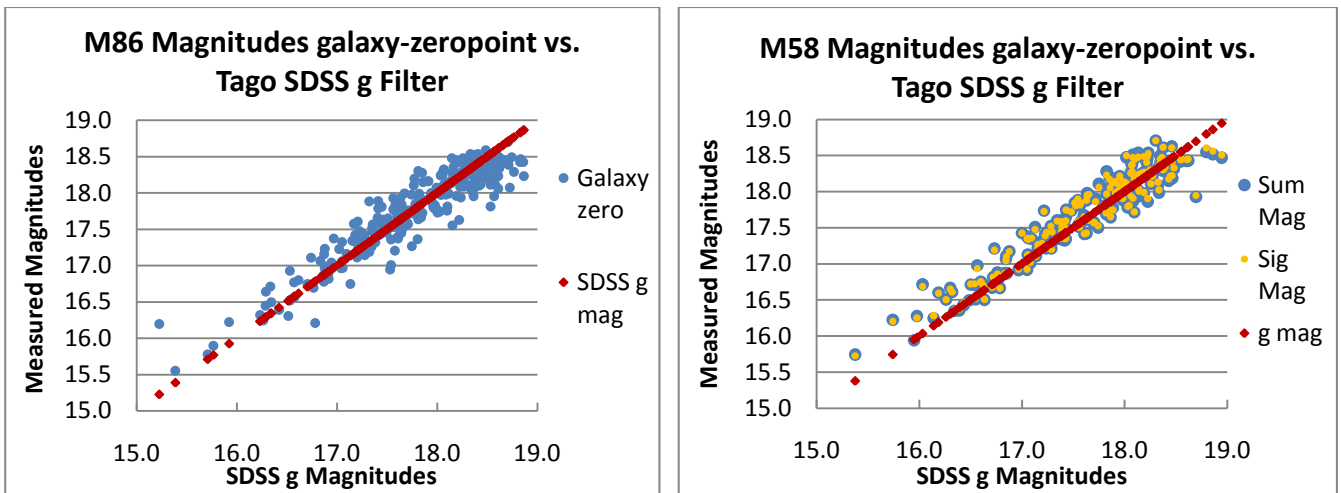


Fig. 10: Comparison of measured magnitudes with Tago (2008) values.

4.3 Collister et al. (2007)

The Collister catalogue (Collister et al. 2007) focused on more distant and fainter galaxies, generally fainter than magnitude 20. It became immediately clear that at these magnitudes, the limits of the system were being reached. For the first time, a significant difference appeared between the two fields. The trendline continued to appear similar to what was seen at brighter magnitudes, showing brighter measurements at fainter magnitudes. Although visual inspection of the cleaned selection showed that the selected objects were indeed the galaxies and not foreground stars or noise, the variance from the

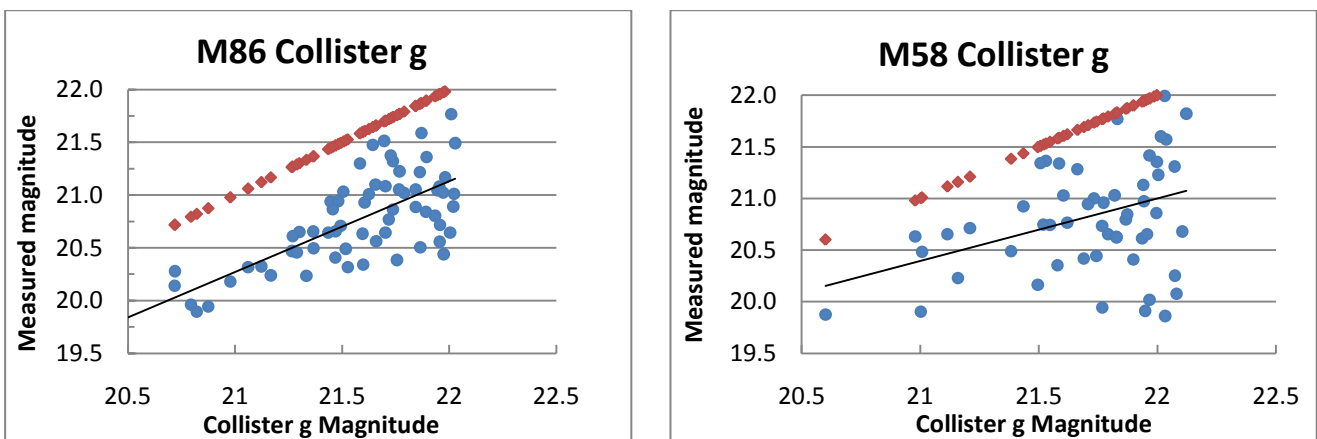


Fig. 11: Comparison of measured magnitudes compared to Collister et al. (2007) for both fields.

measured values, both positive and negative, increased significantly compared to magnitudes ≤ 20 .

However, the variance in the M58f field was clearly higher, as shown in Fig. 11, and in both cases, the errors above magnitude 21.25 increased sharply. At these magnitudes, the S/N ratio is extremely low, generally less than 1, so that even the slight difference in standard deviation in background signal between the two fields became significant.

This can be seen in Fig. 12, where S/N (log scale) is plotted against the measured variance from catalogue magnitude. Galaxies with S/N above 1 showed a generally small, fainter variance from catalogue values, but under 1, the variance increased sharply, first in the direction of the measured magnitudes being brighter than those of the catalogue and then fainter at the lowest S/N ratios. These last are more likely to be false detections. See Appendix 7.3 for a field view of LRG selections.

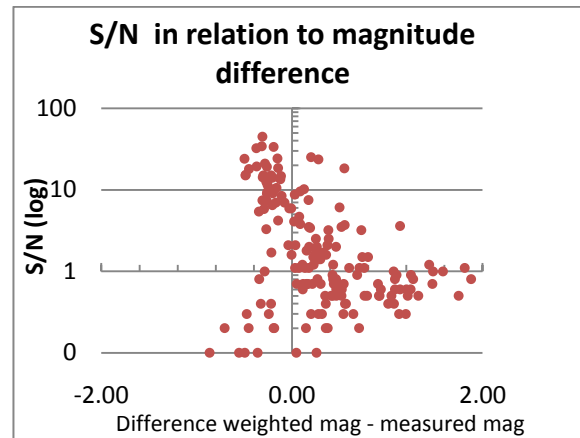


Fig. 12: S/N ratio compared to deviations in magnitude.

4.4 Lopes et al. (2007)

The Lopes et al. (2007) catalogue provided a good check on the preceding results because it combined both high and low magnitudes and high and low redshifts. Again, the difference in magnitude slopes between faint/bright galaxies seen in the VCC and Collister results was repeated. In searching for an explanation, observational data was compared to both the Lopes g and r data. The expectation was that r measurements might prove more accurate for galaxies at higher redshift, due to both redshift and extinction effects (see Fig. 13). Although observed magnitudes were slightly fainter than the r filter magnitudes, the slopes were very similar. If at higher redshifts, the galaxies were indeed redder, then comparing only to the fainter blue magnitudes, while the CCD was also capturing at least a portion of the r passband, could lead to the appearance of an over-estimate of the observed magnitude compared to the Lopes data.

A further analysis of the data showed that galaxies, as measured by Lopes et al. (2007) with g and r filters, did become linearly redder through $z \approx 0.35 - 0.40$, although at $z \approx 0.35$, a break in the trend occurred (Fig. 14a). In addition to the linear relation that was still visible, brighter/bluer galaxies also appeared, but with a less clear trend. This could be caused if nearer galaxies are primarily cluster members and redder ellipticals, while at greater redshifts, more variation in galaxy morphologies, including bluer, starforming spiral field galaxies, might be being measured as well. However, it is beyond the scope of this paper and the available data to draw definite conclusions on this point. Magnitude, certainly up to $z \approx 0.40$, is to a great extent linked to redshift (Fig. 14d). However, the S/N ratio degraded around the same $z \approx 0.35 -$

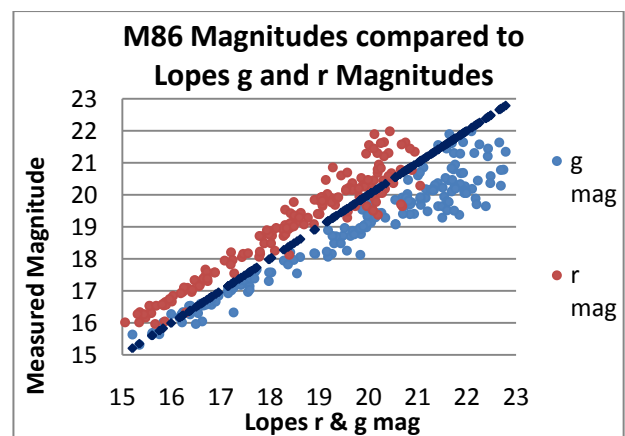


Fig. 13: Observed magnitudes compared to Lopes r and g magnitudes.

0.40 limit (Fig. 14b), leading to a greater possibility errors in the measurements.

It is interesting to note that even the higher-resolution SDSS data shows two of the same trends as the observational data: more variation from a mean at high red-shift, and, if a trendline is drawn through the entire range of data, slightly fainter measurements at low redshifts and brighter at higher redshifts, although this trend is clearly stronger in the observational data than for published values.

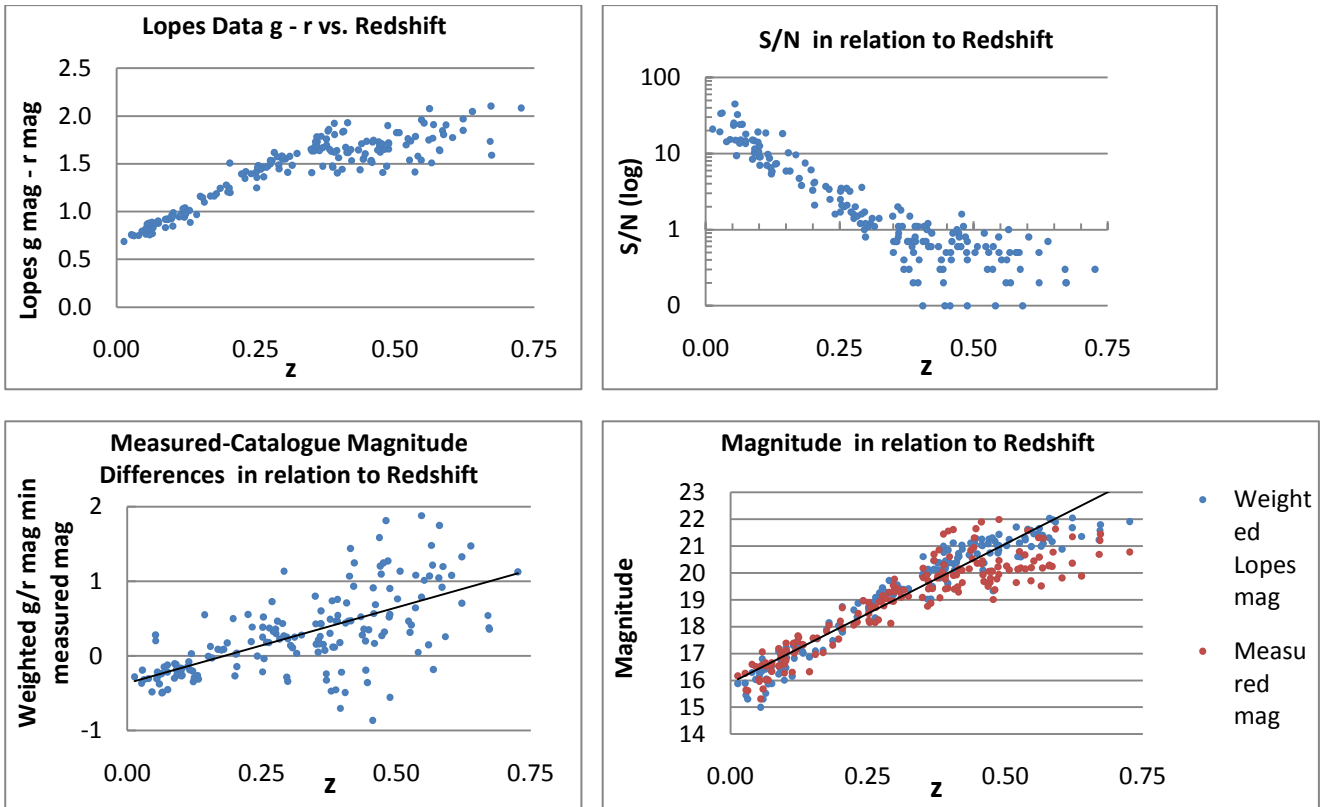


Fig. 14: a) above left, Lopes g - r color vs. redshift; b) above right, S/N vs. redshift, c) below left, magnitude variances vs. redshift and d) magnitude vs. redshift.

Since the filter response profile shows that the M25c CCD covers the entire g and a portion of the r filter, a weighted magnitude was calculated using the formula $((3 * g) + (2 * r))/5$ to better approximate the contribution of both filters. As can be seen in Fig. 15, this weighted average produced a better fit to the Lopes data and a similar result to that of the VCC visual magnitudes.

Further comparisons of magnitude and redshift on the Lopes data confirmed the conclusions from the VCC, Tago and Collister data concerning the limits of the system. Weighted measurements closely follow published values up to $z \approx 0.35 - 0.40$ / magnitude ≈ 20 . However, after $z \geq 0.37$ / magnitude ≈ 21 , although galaxies can be correctly identified, the accuracy of the measurements becomes less certain, with a slight tendency to overestimate the brightness at higher z. Not surprisingly, this uncertainty is

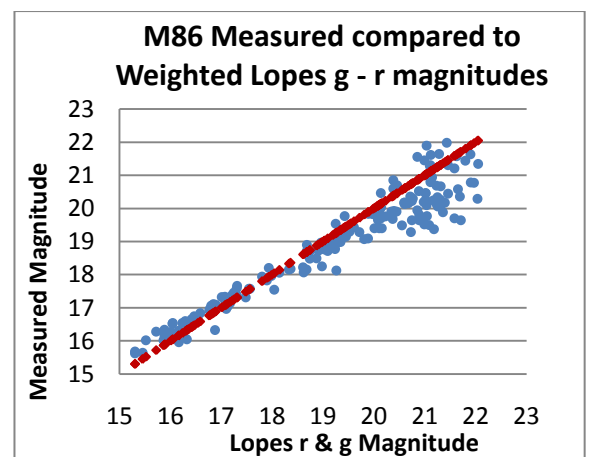


Fig. 15: Measured magnitudes compared to a weighted average of the Lopes g and r filters.

at least in part linked to the sharp decrease in S/N ratio that occurs at about the same z .

4.5 Lisker et al. (2006, 2007)

One final area of interest was the level of detail that can be seen in the smaller galaxies. As resolution has increased over time, it has become clear that at least some galaxies previously described only as dwarf elliptical (dE) or SO did in fact show disks, structure, bluer colors or other features (Lisker et al. 2006).

A sub-classification within the dEs was constructed to include dE(di) = disks, dE(bc)= blue center, dE(N)= nucleated and dE(nN) = non-nucleated (Lisker et al. 2007). In addition, a classification of faint (ft) or bright (bt) was given. According to Lisker et al. (2007), the dwarfs showing disk features or blue centers and the bright non-nucleated dwarfs resemble thick disks and may show evidence of recent mergers and star formation. The bright and faint nucleated galaxies should be more spheroid, although still somewhat oblate, and are to some extent smaller versions of the larger ellipticals around which they generally are clustered.

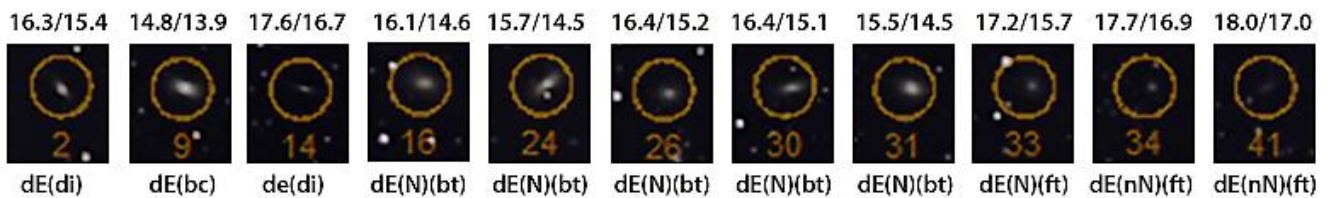


Fig. 16: Selection of galaxies, magnified to 200%, showing comparison with Lisker et al. morphologies and Lisker/observed magnitudes.

A sample was examined from the Lisker database, shown above at 200% magnification (see Appendix 7.4 for view of field selection). Flattened shapes in the di and bc galaxies are clearly seen. dEs 16, 24 and 30 also seem to show much more of a flattened disk that suggested by the Lisker description. However, it was found that in general, with this imaging set-up and exposure times, variations in shape and surface brightness could be observed to \approx magnitude 17 - 18. Above that, the galaxies were too faint and/or too small to be certain of their characteristics.

5 Summary and conclusions

It would appear that a fairly modest amateur telescope and CCD camera can at least identify faint galaxies of magnitudes ≤ 22 à 23. Through magnitude 19 – 20, measurements of these galaxies show a high degree of accuracy. However, above magnitude 20.5 and $z \approx 0.35 - 0.40$, where S/N ratios become low, measurements show a higher spread in comparison published data, generally tending to have brighter measured magnitudes than catalogue magnitudes. The image with a shorter exposure time showed similar good results at brighter magnitudes ≤ 20 , but greater variance from published data at magnitudes ≥ 20 . As magnitudes become fainter and z increases, it becomes increasingly important to match filters and CCD sensitivity.

While the results of these observations were encouraging, the accuracy of the measurements can be significantly improved by the use of photometric filters and a monochrome, non-anti-blooming CCD camera. It would also be interesting to photometrically examine the color of the more distant galaxies

to see if the same trend can be observed as shown in Fig. 14a. Finally, it would be interesting to see if longer exposures and/or higher resolution would improve the scatter seen in the distant galaxies.

6 References

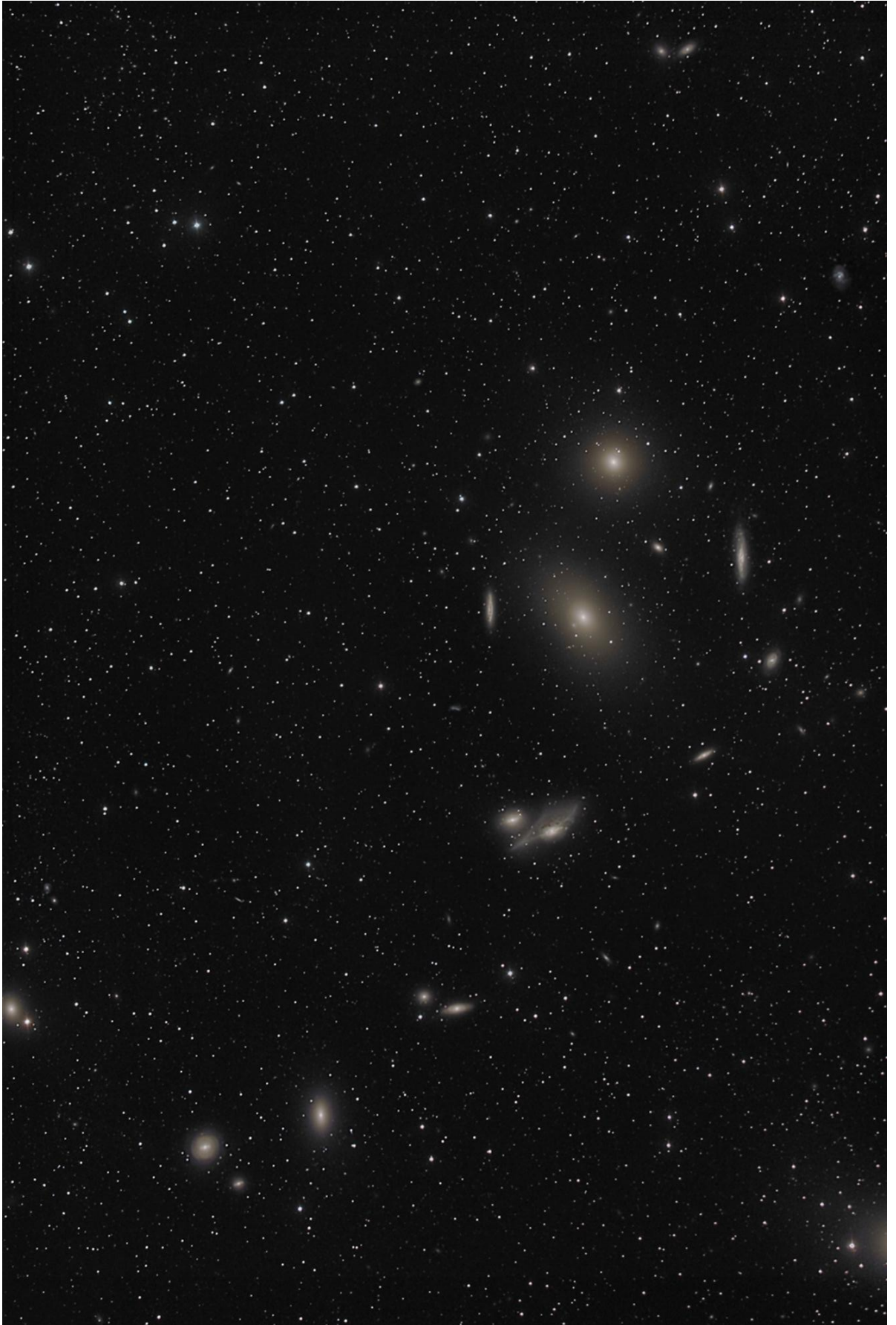
- Adelman-McCarthy, J. K. et al. 2007, *ApJS*, 172, 634
Adelman-McCarthy, J. K. et al. 2006, *ApJS*, 162, 38
ATiK-web: ATiK CCD Cameras and Accessories, <http://www.telescope-service.com/atik/start/atikstart.html#2HS> (accessed 2 June 2010)
Binggeli, B., & Huchra, J. P. 2001, in *EAA* (Hampshire, UK: IOP Publishing Ltd)
Binggeli, B., Sandage, A., & Tammann, G. A. 1985, *AJ*, 90, 1681
Celestron-web: DISCONTINUED: NexStar 11 GPS Computerized Telescope, <http://www.celestron.com/c3/product.php?ProdID=78> (accessed 2 June 2010)
Ciardullo, R., Jacoby, G. H., & Ford, H. C. 1989, *AJ*, 344, 715
Collister, A. et al. 2007, *MNRAS*, 375, 68
Lisker, T., Grebel, E. K., & Binggeli, B. 2006, *AJ*, 132, 497
Lisker, T., Grebel, E. K., Binggeli, B., & Glatt, K. 2007, *AJ*, 660, 1186
Lopes, P. A. A. 2007, *MNRAS*, 380, 1608
Maxim-web: Cyanogen Imaging Products from Diffraction Limited, http://www.cyanogen.com/maxim_main.php (accessed 20 May 2010)
Mira-web: Mirametrics, <http://www.mirametrics.com/index.htm> (accessed 20 May 2010)
Sandage, A., & Tammann, G. A. 2006, *ApJ*, submitted
Smith, S. 1936, *ApJ*, 83, 23
Starlight-web: Starlight XPress SXV series cameras, <http://www.starlight-xpress.co.uk/SXV-M25.htm> (accessed 2 June 2010)
Stellarvue-web: Nighthawk Next Generation Deluxe - Stellarvue Telescopes by Stellarvue, <http://www.stellarvue.com/sv80ed.html> (accessed 2 June 2010)
Tago, E., Einasto, J., Saar, E., Tempel, E., Einasto, M., Vennik, J., & Müller, V. 2008, *A&A*, 479(3), 927
Tucker, S. 2008, *Astronomy Technology Today*, 2(10), 29
van Gastel, J. 2010, private communication
Villegas, D. et al. 2010, *ApJ*, accepted
Zwicky, F. 1937, *ApJ*, 86, 217

7 Appendix

7.1 Reduction log (sent as separate word document)

7.2 Color field images

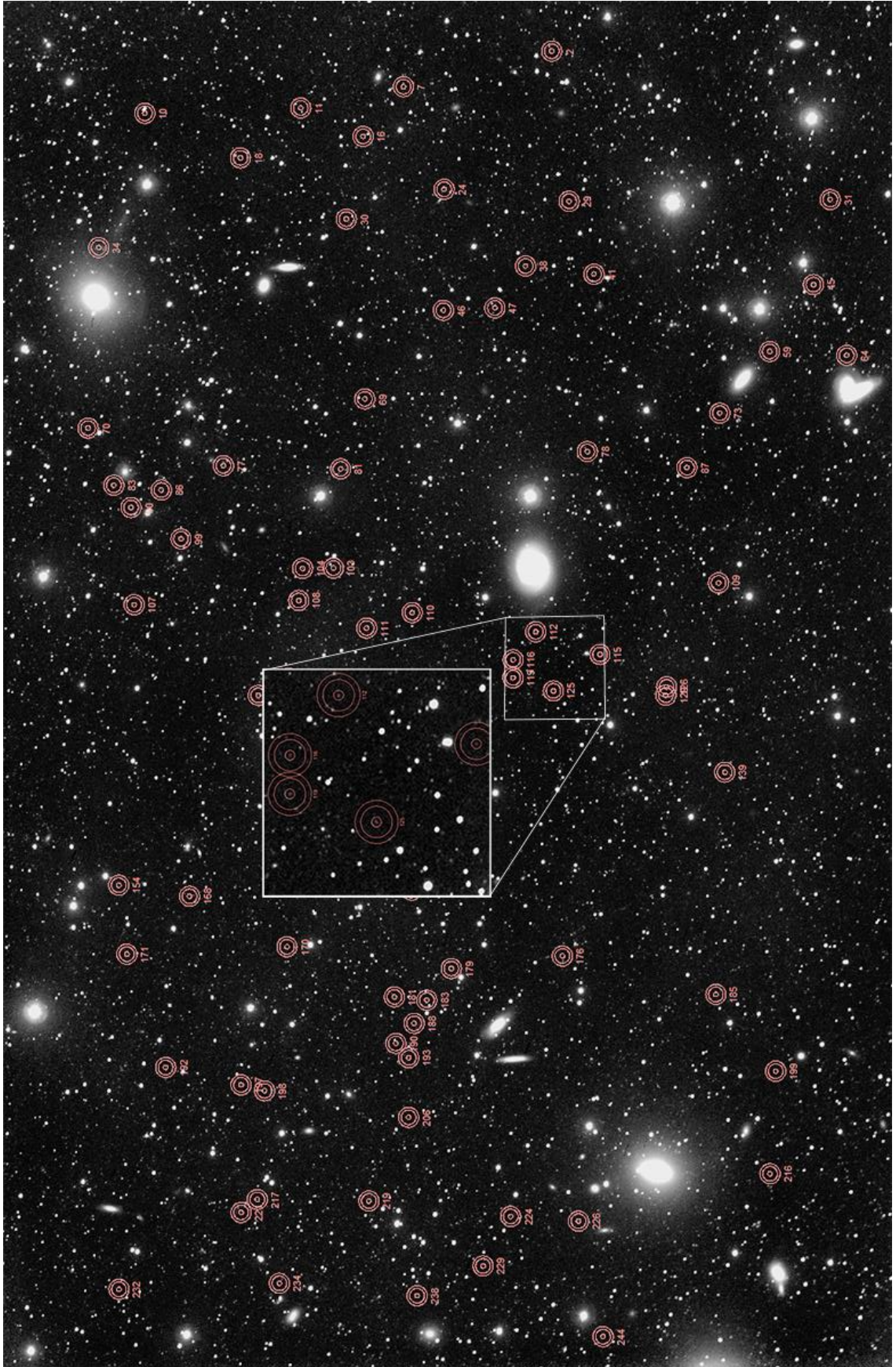
7.2.1 M86f color image



7.2.2 M58f color image



7.3 M58f with LRG selection



7.4 M86f with Lisker et al. (2006, 2007) dE selection

